Heliyon 10 (2024) e34000

Contents lists available at ScienceDirect

Heliyon

journal homepage: www.cell.com/heliyon

Research article

Green synthesized extracts/Au complex of *Phyllospongia lamellosa*: Unrevealing the anti-cancer and anti-bacterial potentialities, supported by metabolomics and molecular modeling

Sultan Aati [a,**,1], Hanan Y. Aati [b,1], Sherine El-Shamy [c], Mohammad A. Khanfar [d], Mohamed A.Ghani A.Naeim [e], Ahmed A. Hamed [f], Mostafa E. Rateb [g], Hossam M. Hassan [h,i,*], Mahmoud A. Aboseada [i]

[a] *Dental Health Department, College of Applied Medical Sciences, King Saud University, Riyadh, Saudi Arabia*
[b] *Department of Pharmacognosy, College of Pharmacy, King Saud University, Riyadh, 11495, Saudi Arabia*
[c] *Pharmacognosy Department, Faculty of Pharmacy, Modern University for Technology and Information, Cairo, Egypt*
[d] *Department of Pharmaceutical Sciences, Faculty of Pharmacy, The University of Jordan, P.O Box 13140, Amman, 11942, Jordan*
[e] *Environmental Researcher Red Sea Marine Park, Egypt*
[f] *National Research Centre, Microbial Chemistry Department, 33 El-Buhouth Street, Dokki, Giza, 12622, Egypt*
[g] *School of Computing, Engineering & Physical Sciences, University of the West of Scotland, Paisley, PA1 2BE, Scotland, UK*
[h] *Department of Pharmacognosy, Faculty of Pharmacy, Beni-Suef University, Beni-Suef, Egypt*
[i] *Department of Pharmacognosy, Faculty of Pharmacy, Nahda University, Beni-Suef, Egypt*

ARTICLE INFO

Keywords:
Phyllospongia lamellosa
Gold nanoparticles
Metabolomics
Anti-Cancer
Anti-Bacterial
Molecular docking

ABSTRACT

The anti-cancer and anti-bacterial potential of the Red Sea sponge *Phyllospongia lamellosa* in its bulk (crude extracts) and gold nanostructure (loaded on gold nanaoparticles) were investigated. Metabolomics analysis was conducted, and subsequently, molecular modeling studies were conducted to explore and anticipate the *P. lamellosa* secondary metabolites and their potential target for their various bioactivities. The chloroformic extract (CE) and ethyl acetate extract (EE) of the *P. lamellosa* predicted to include bioactive lipophilic and moderately polar metabolites, respectively, were used to synthesize gold nanoparticles (AuNPs). The prepared AuNPs were characterized through transmission electron microscopy (TEM), Fourier-transform infrared spectroscopy (FTIR), and UV–vis spectrophotometric analyses. The cytotoxic activities were tested against MCF-7, MDB-231, and MCF-10A. Moreover, the anti-bacterial, antifungal, and anti-biofilm activity were assessed. Definite classes of metabolites were identified in CE (terpenoids) and EE (brominated phenyl ethers and sulfated fatty amides). Molecular modeling involving docking and molecular dynamics identified Protein-tyrosine phosphatase 1B (PTP1B) as a potential target for the anti-cancer activities of terpenoids. Moreover, CE exhibited the most powerful activity against breast cancer cell lines, matching our molecular modeling study. On the other hand, only EE was demonstrated to possess powerful anti-bacterial and anti-biofilm activity against *Escherichia coli*. In conclusion, depending on their bioactive metabolites, *P. lamellosa*-

* Corresponding author. Department of Pharmacognosy, Faculty of Pharmacy, Beni-Suef University, Beni-Suef, Egypt.
** Corresponding author.
E-mail addresses: Sati@ksu.edu.sa (S. Aati), hati@ksu.edu.sa (H.Y. Aati), s_elshamy@hotmail.com (S. El-Shamy), mabdelghany@hotmail.com (M.A. Khanfar), ahmedshalbio@gmail.com (A.A. Hamed), mostafa.rateb@uws.ac.uk (M.E. Rateb), hossam.mokhtar@nub.edu.eg (H.M. Hassan), mahmoud.moawwad@nub.edu.eg (M.A. Aboseada).
[1] those authors are equally contributed.

https://doi.org/10.1016/j.heliyon.2024.e34000
Received 11 April 2024; Received in revised form 2 June 2024; Accepted 2 July 2024
Available online 2 July 2024
2405-8440/© 2024 The Authors. Published by Elsevier Ltd. This is an open access article under the CC BY-NC license (http://creativecommons.org/licenses/by-nc/4.0/).

derived extracts, after being loaded on AuNPs, could be considered anti-cancer, anti-bacterial, and anti-biofilm bioactive products. Future work should be completed to produce drug leads.

1. Introduction

Cancer is a disease that causes pathophysiological abnormalities in the intrinsic process of cellular division. It has become a substantial health issue responsible for a high number of fatalities annually on a global scale [1,2]. In 2020, more than 19.3 million newly diagnosed cases of cancer were identified, and this would result in roughly 10 million mortalities [3]. The necessity and demand for creating powerful medications to treat various malignancies have been fueled by the global increasing prevalence of cancer cases, which result in millions of deaths each year [4–8]. Globally, breast cancer ranks as the second most common cause of mortality experienced by women. The medicinal therapy of this disease is greatly hampered by its heterogeneity. However, recent advances in immunology and molecular biology enable the development of highly specialized therapies for various breast cancer types [9].

Antibiotic resistance is a major worldwide health threat that presents a considerable obstacle to effectively treating infectious diseases. Antibiotic-resistant bacteria have disseminated due to the inappropriate and excessive use of antibiotics, raising morbidity, death, and healthcare expenditures worldwide [10–13].

Natural products with established human consumption include dietary phytochemicals, nutritional herbs, and bioactive components. There is no evidence of systemic toxicity or hazardous side effects in these products. Due to these merits, natural products have the potential to serve as viable substitutes for treatment-resistant breast cancer. On the other hand, none of the recently produced antibiotics are anticipated to be effective against the harmful strains of antibiotic-resistant bacteria, notwithstanding the diligent endeavors. The desire for herbal remedies to co-treat antibiotic-resistant microorganisms has lately surged. It has been evidenced that numerous natural products have been discovered to possess potent antimicrobial components that can work either alternately or synergistically with antibiotics [14–18].

Marine ecosystems are exceptionally diverse and home to various unusual living forms that may have distinctive chemical and biological characteristics, imparting significant therapeutic applications. Sponges are among the most promising aquatic creatures because of their exceptional biological activity and previously unheard-of sophisticated chemistry [19].

Consequently, this research aimed to determine whether a crude organic extract obtained from the marine sponge *Phyllospongia lamellosa* could be utilized to produce bioactive and stable AuNPs. According to earlier reports, *P. lamellosa* is an excellent source of bioactive chemicals, especially sesterterpenes, which have demonstrated extremely promising anti-cancer activities [20–22]. The AuNPs of *P. lamellosa* extracts were examined for their anti-microbial and anti-breast cancer properties.

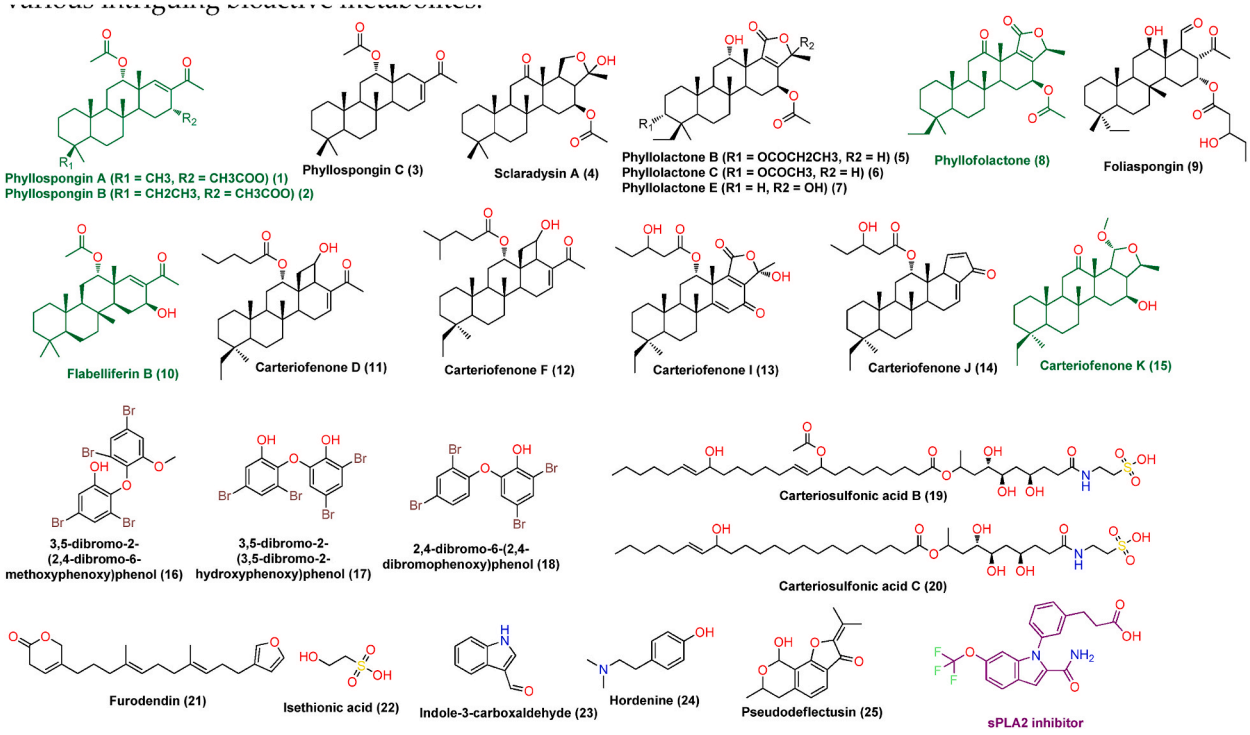

Fig. 1. Chemical structures of compounds 1–25 that have been putatively identified in the *P. lamellosa*-derived extracts, CE and EE.

2. Results and discussion

2.1. Chemical profiling of P. lamellosa-derived extracts

P. lamellosa-derived extracts were chemically characterized, leading to the tentative identification of 25 major compounds (high features), ranked by peak intensities (Table S1, Fig. 1). The identified compounds (1–15) in CE were found comprising the terpenoids class of natural products (i.e., sesterterpenes and triterpenes), while in the EE, three brominated aromatic ethers (16–18), two sulfated fatty amides (19 and 20), in addition to other five miscellaneous compounds (21–25) were identified. All identified compounds have previously been reported from P. lamellosa or other species of Phyllospongia [20–22]. P. lamellosa is particularly known for its sesterterpenes and triterpenes (1–15), which have been demonstrated to have intriguing anticancer potential against various human cancer cell lines [20,23,24]. Furthermore, they demonstrated moderate antiviral and anti-inflammatory efficacy in both in vitro and in vivo designs [20–22].

Two examples of sulfated fatty amides were detected in the EE (19 and 20, respectively), namely carteriosulfonic acid B and C. Both of these compounds have been reported to inhibit glycogen synthase kinase-3 beta (GSK-3β)in vitro; hence, they are considered very potential therapeutic candidates for managing type 2 diabetes mellitus [25]. There is promising evidence that optimizing the biological activity of gold nanoparticles (AuNPs) can be achieved by loading such crude extract abundant in various intriguing bioactive metabolites.

3. *P. lamellosa*-containing AuNPs

3.1. Biosynthesis of AuNPs using CE and EE of P. lamellosa

The synthesis of AuNPs using CE and EE was done by mixing 10 mL of 10^{-3} M $HAuCl_4$ aqueous solution with 1 mL of 0.010 g of each extract. The reduction process was at room temperature with stirring. The reaction's color change was visually assessed, and the transition duration was documented. The creation of gold nanoparticles is signified by an instantaneous shift in the solution's color from light pale yellow to dark purple in EE or from pale brownish to purple in CE (Fig. 2a and c). After mixture centrifuging for 20 min, the resulting pellet was rinsed with de-ionized water to eliminate contaminants. A triplicate cycle of centrifugation and rinsing was executed to obtain a more effective separation of nanoparticles. The resulting AuNPs were maintained at 4 °C after being oven-dried for 5 h at 45 °C.

3.2. Electron microscopy

Field emission scanning electron microscopy (FESEM) and transmission electron microscopy (TEM) techniques were utilized to evaluate the particle size and morphology of the green-produced AuNPs. The TEM micrograph showed that the average particle size for the AuNPs formed by CE was about ~4.68 ± 2 to 23 ± 74 nm with monodisperse spherical-like shapes. The average particle size for the AuNPs formed by EE was about ~6.04 ± 2 to 21 ± 2 nm with hexagonal prism-like shapes (Fig. 3a and c and Fig. 4).

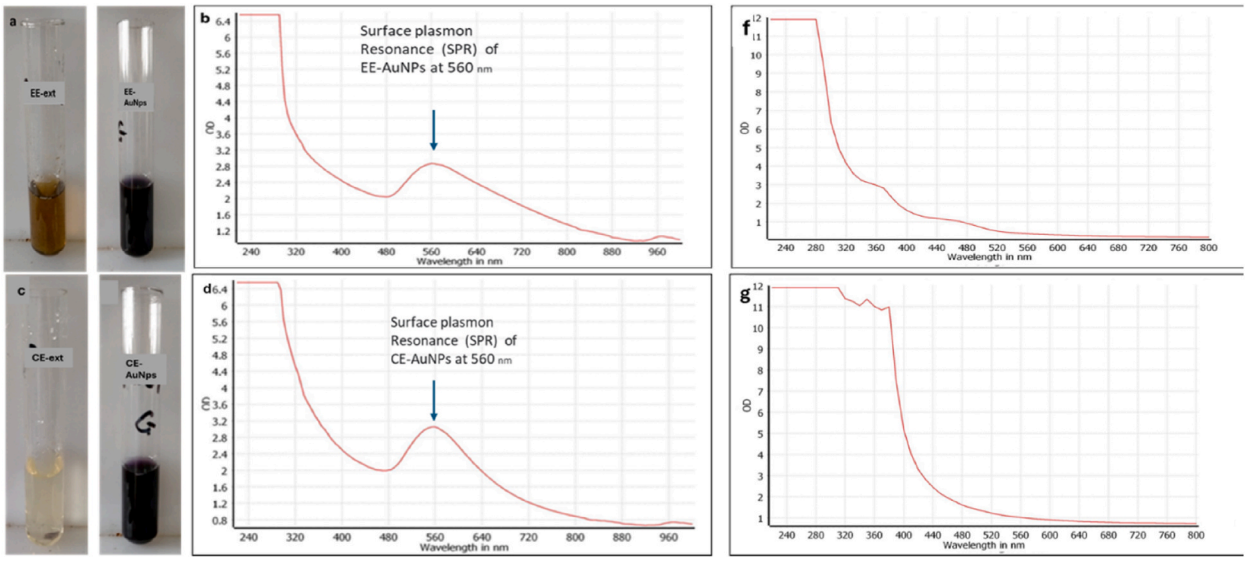

Fig. 2. Color change due to formation of AuNPs by CE (a) and EE (c) and UV–vis spectra showing a clear plasmon band for Au-NPs synthesized by CE (b) and EE (d). While (f) is the crude of EE and (g) is the crude of CE. (For interpretation of the references to color in this figure legend, the reader is referred to the Web version of this article.)

3.3. X-ray powder diffraction (XRD)

XRD spectroscopy of the synthesized gold nanoparticles by CE demonstrated the presence of distinguishing peaks of gold at 38°, 44°, and 66° (Fig. 5), accredited to the crystallographic planes (111), (200), and (220) of gold. Concerning the synthesized gold nanoparticles by EE, the XRD patterns for gold nanoparticles between 2θ of 20–80° are noticed. XRD configurations demonstrate the diffraction peaks of gold nanoparticles at 2θ values for 38°, 44°, and 65.37°, which matched with 111, 200, and 220 crystallographic planes.

3.4. Fourier transforms infrared spectroscopy analysis (FTIR)

The FTIR was achieved to detect the functional groups responsible for stabilizing and synthesizing gold nanoparticles. The FTIR spectral profile of the green AuNPs prepared by CE and EE extracts, along with the FTIR of both extracts, was measured at the wavelength range of 4000–450 cm^{-1}, showing that hydroxyl group (O–H) stretching vibration appears at 3329.86 cm^{-1} in CE and 3442.19 cm−1in EE. In contrast, peaks appeared at 2920.34, and 2850.57 cm^{-1} in CE and 2963.50 cm^{-1} in EE refers to the alkane (C–H) stretching vibrations. Moreover, the aromatic (C═C) stretch vibration was demonstrated at 1635.94 cm^{-1} in CE. The C–O was measured at 1419.67 in CE and at 1414.78 and 1384.76 cm^{-1} in EE, and the bands at 1197.80 and 1180.79 cm^{-1} in CE and from 1303.54: 1154.77 in EE refer to C–N stretching. Furthermore, the C–C appears at 1036.91 cm^{-1} in CE and around 1077.82 cm^{-1} in EE. Finally, the IR peak at 1649.88 cm^{-1} is due to the (C═O) present in the EE extract. These functional groups, for instance, nitrogenous, carboxyl, and hydroxyl groups, interact with the gold metal ion and reduce it to AuNPs (Fig. 6). It also serves a critical role in stabilizing AuNPs (Fig. 6).

3.5. In vitro cytotoxic activity of AuNPs-loaded P. lamellosa extracts

Nanotechnology offers the means to target therapies directly and selectively to cancerous cells and neoplasms. Nanotechnology is also presents a unique set of tools to overcome drug resistance and deliver drugs across traditional biological barriers and combines therapeutic agents with imaging techniques towards achieving synergic results [26–28]. Therefore, the synthesized AuNPs loaded with those extracts suggested substantial potential to be more effective than free Au and non-loaded extracts. Accordingly, we conducted experiments on the papered AuNPs against two human breast cancer cell lines, multidrug-resistant invasive ductal (MDA-MB-231) and estrogen-positive metastatic (MCF-7), as well as against normal breast cells (MCF-10a), to assess the toxicity of these AuNPs.

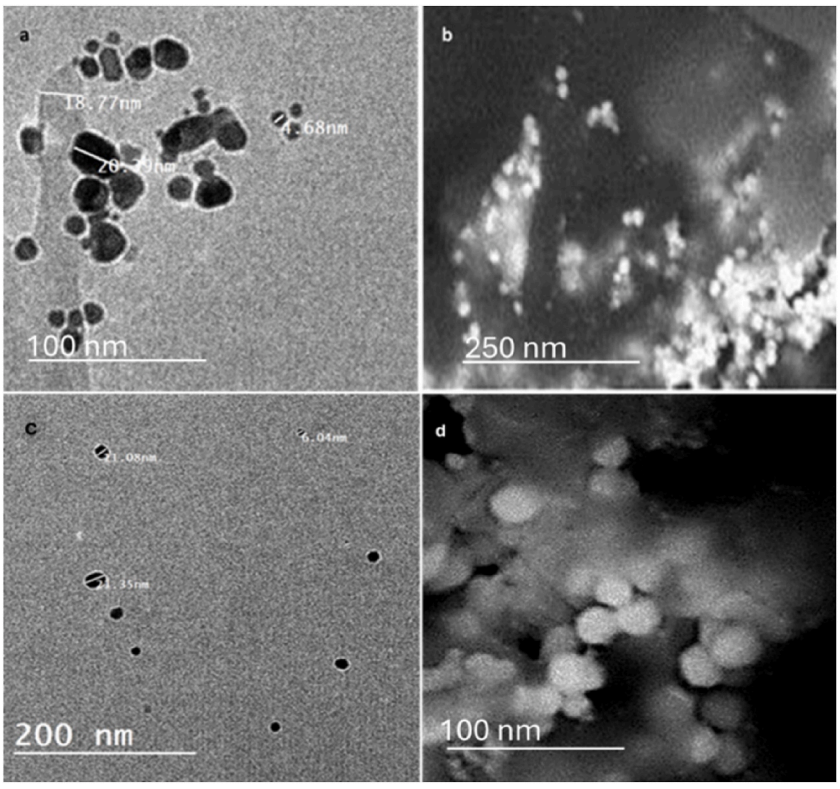

Fig. 3. TEM micrographs of poly-dispersed-shaped AuNPs prepared with CE (a) and spherical-shaped AuNPs prepared with EE (c) and FESEM micrographs of the prepared AuNPs (b,d).

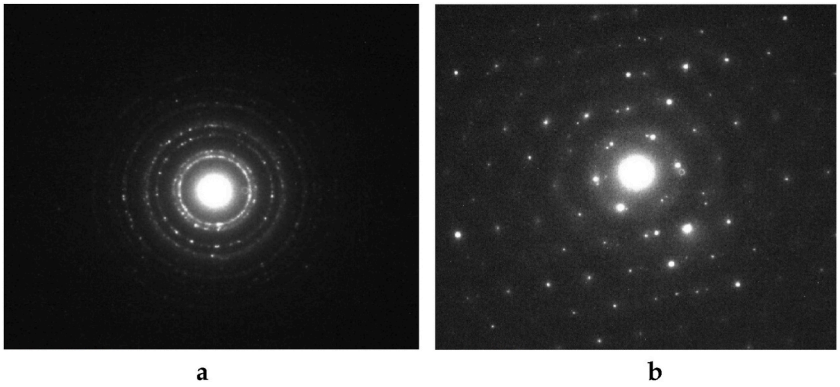

Fig. 4. Selected area diffraction (SAED) images for prepared AuNPs using CE (a) and EE (b).

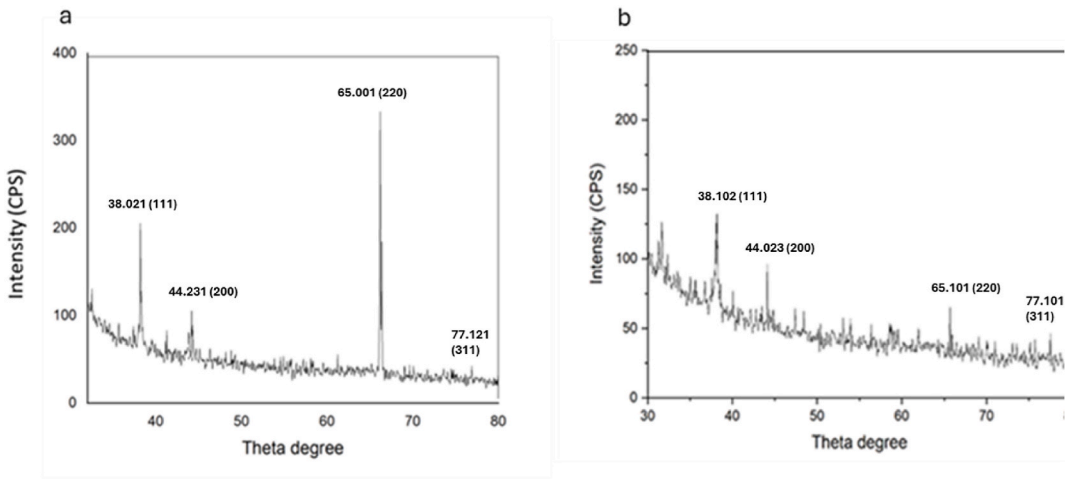

Fig. 5. X-ray diffraction pattern of the gold nanoparticles prepared by a) CE and b) EE.

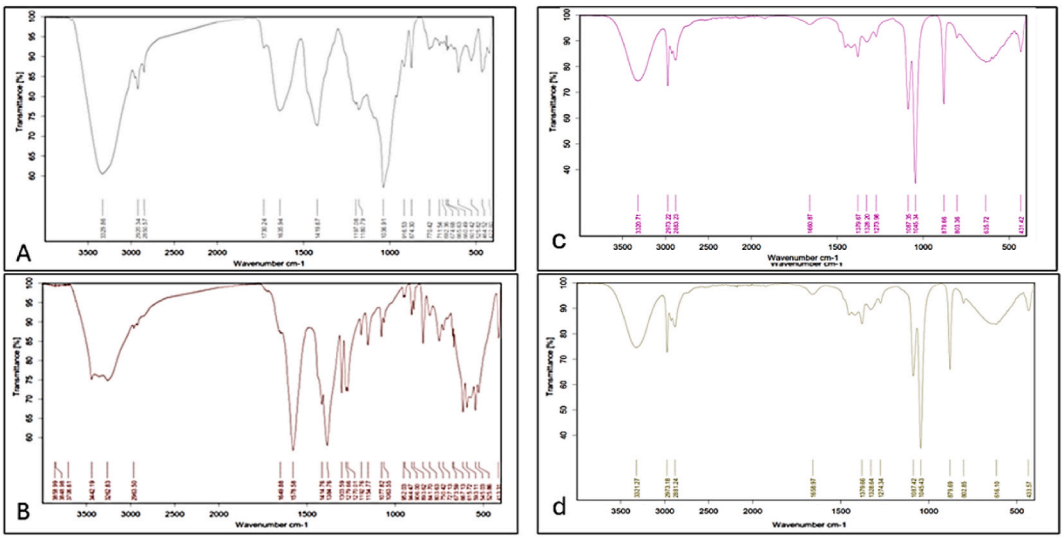

Fig. 6. FTIR spectra of the green prepared AuNPs using a) CE and b) EE extracts, c) crude of CE and d) crude of EE. (For interpretation of the references to color in this figure legend, the reader is referred to the Web version of this article.)

As shown in Table 1, both AuNPs loaded with CE (CE-AuNPs) and EE (EE-AuNPs) exhibited remarkable inhibitory action towards MCF-7 (IC_{50} = 8.2 ± 0.38 and 10.2 ± 0.47 μg/mL, respectively). They exhibited considerably greater efficacy than free ones (IC_{50} = 93.9 ± 4.35 μg/mL). Similarly, CE-AuNPs and EE-AuNPs exerted more powerful inhibitory action towards MCF-7 than non-loaded ones (IC_{50} = 26.6 ± 1.0 (CE) and 36 ± 1.4 (EE) μg/mL, respectively). Concerning MDA-MB-231, the Au significantly showed lower cytotoxicity (IC_{50} = 25.4 ± 0.12 μg/mL) than those loaded with extracts (IC_{50} = 12.9 ± 0.6 and 13.3 ± 0.62 μg/mL, concerning EE-AuNPs and CE-AuNPs, respectively).

Interestingly, compared to the reference medication, Taxol (IC_{50} = 12.47 ± 1.25 μg/mL), CE-AuNPs and EE-AuNPs exhibited higher potency, and this suggests the probable potential of brominated aromatic ethers (16–18) and sulfated fatty amides (19 and 20) identified in EE, as well as sesterterpenes and triterpenes (**1–15**) identified in CE as potent anticancer agents. In detail, Carteriosulfonic acids B and C (19 and 20) were reported to inhibit GSK-3β in a ^{32}P-labeling assay with IC_{50} values of 6.8 and 6.8 μM, respectively [25,29]. GSK-3β inhibitors were suggested as promising targets in cancer treatment [25,30]. Furthermore, polybrominated diphenyl ethers such as those identified in EE (16–18) were proved to be ones of promising anticancer drugs [31]. In general, a plethora of marine-identified brominated phenols or brominated diphenyl ethers have been investigated for their cytotoxic activity, impacting powerful anticancer potentiality. Morover, sesterterpenes and triterpenes (**1–15**) identified in CE, have been demonstrated to possess intriguing anticancer potential against various human cancer cell lines [20,23,24].

The toxicity of prepared CE-AuNPs toward normal breast cell lines was highly weak (IC_{50} 186 ± 8.61 μg/mL) compared with that of Taxol (37.24 ± 1.67 μg/mL), indicating the remarkable safety of CE-AuNPs (see Table 1).

According to these findings, the chemical components mentioned above in P. lamellosa-derived extracts, CE and EE, exhibited a noteworthy inhibitory impact on both estrogen-sensitive and multidrug-resistant invasive ductal breast cancer cells and boosted the effectiveness of AuNPs with lesser cytotoxicity. In general, they even attempted to increase the enhanced effectiveness of the free AuNPs with high marginal safety.

3.6. Antibacterial activity of AuNPs-loaded P. lamellosa extracts

Compared to the positive control ciprofloxacin, the bacterial inhibition results for CE-AuNPs and EE-AuNPs show varied activity patterns against different bacterial strains. CE-AuNPs showed a minor bacterial inhibition against *Staphylococcus aureus* and *Salmonella typhi*, while EE-AuNPs had moderate activity towards *S. typhi*. On the other hand, CE-AuNPs had a weak anti-bacterial effect against *Proteus* sp., while EE-AuNPs showed no effect. Concerning *E. Coli*, both extracts were potentially active with an inhibition percent comparable to the positive control, which clarifies the effect of different metabolites in both extracts. (Fig. 7a and 6b). Numerous types of those metabolites were reported to exhibit anti-bacterial activity. By CE, phyllospongins, namely phyllospongins D and E (structurally related to phyllospongins A-C; 1–3), were previously reported to exhibit significant anti-bacterial potential against *S. aureus*, *Vibrio parahaemolyticus*, and *Bacillus subtilis*; recording MIC values = ~1.7–3.3 μg/mL [21,32]. On the other hand, 2,4-dibromo-6-(2, 4-dibromophenoxy)phenol (18) identified in EE was demonstrated to display activities against *B. subtilis*, *S. aureus*, *Klebsiella Pneumoniae*, and *E. coli* with MIC values ranging from 0.5 to 6.3 Mm [33].

3.7. Antifungal activity of AuNPs-loaded P. lamellosa extracts

Testing both extracts for their antifungal activities against *Aspergillus niger* and *Candida albicans* showed that the CE-AuNPs had a higher effect than the EE-AuNPs, as they showed moderate activity while EE-AuNPs showed weak activity (Fig. 8a & b).

3.8. Biofilm inhibitory activity of AuNPs-loaded P. lamellosa extracts

The biofilm inhibition results of CE-AuNPs against the investigated microorganisms provided exciting information about their potential as an antibacterial agent. *S. aureus*, a common pathogen known to generate biofilms, did not respond to CE-AuNPs, indicating a lack of inhibitory action. This showed that either the nanoparticles were ineffective against this strain or the concentration used in the study was insufficient to suppress biofilm. In contrast, *S. typhi*. showed a moderate biofilm inhibition percentage of 30.69 % in

Table 1
In vitro growth inhibitory activity of the prepared AuNPs against estrogen-positive and triple-negative breast cancer cell lines alongside normal breast cell line.

Sample	Cytotoxicity IC_{50} μg/mL		
Code	MCF7	MDA-MB-231	MCF10a
CE	26.6 ± 1.0	10.1 ± 0.4	13.1 ± 0.5
EE	36 ± 1.4	17.2 ± 0.7	30.3 ± 1.1
CE-AuNPs	8.2 ± 0.38	13.3 ± 0.62	186 ± 8.61
EE-AuNPs	10.2 ± 0.47	12.9 ± 0.6	47.4 ± 2.2
Au	93.9 ± 4.35	25.4 ± 0.12	25.9 ± 1.2
Taxol **	12.47 ± 1.25	15.39 ± 0.84	37.24 ± 1.67

AU: Gold metal, **CE-AuNPs**: Chloroformic extract loaded on gold nanoparticles, **EE-AuNPs**: Ethyl acetate extract loaded on gold nanoparticles, **MCF7**: Estrogen-positive metastatic cell lines, **MDA-MB-231**: Multidrug-resistant invasive ductal cell lines, **MCF10a**: Normal breast cell lines, and **: Positive control.

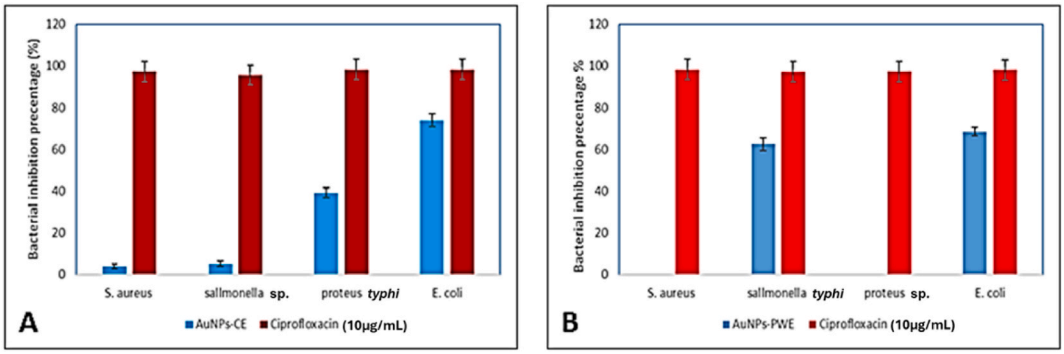

Fig. 7. Bacterial inhibition percentage of a) CE-AuNPs and b) EE-AuNPs. **CE-AuNPs**: Chloroformic extract loaded on gold nanoparticles, **EE-AuNPs**: Ethyl acetate extract loaded on gold nanoparticles, ***S. aureus***: **Staphylococcus aureus**, ***E. coli***: *Escherichia coli*. (For interpretation of the references to color in this figure legend, the reader is referred to the Web version of this article.)

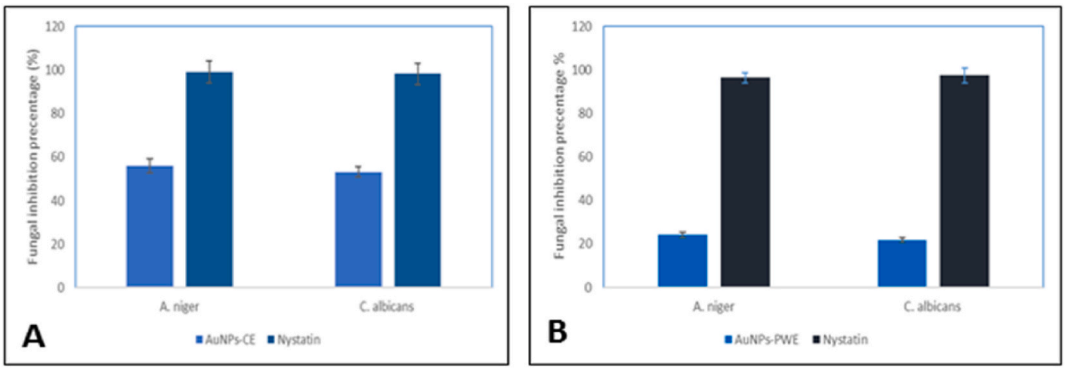

Fig. 8. Fungal inhibition percentage of a) CE-AuNPs and b) EE-AuNPs. ***A. niger***: *Aspergillus niger*, ***C. albicans***: *Candida albicans*, **CE-AuNPs**: Chloroformic extract loaded on gold nanoparticles, **EE-AuNPs**: Ethyl acetate extract loaded on gold nanoparticles. (For interpretation of the references to color in this figure legend, the reader is referred to the Web version of this article.)

response to CE-AuNPs. This finding implies a possible efficacy in reducing Salmonella biofilm development. In contrast, *Proteus* spp. showed no biofilm inhibitory activity in the presence of CE-AuNPs. *E. coli*, another prevalent pathogenic bacterium, exhibited a modest biofilm inhibitory percentage of 19.71 % in response to CE-AuNPs (Table 2).

The biofilm inhibitory results for EE-AuNPs against various bacterial strains offer valuable insights into its potential as an agent for combating biofilm formation. Starting with *S. aureus*, EE-AuNPs exhibited a biofilm inhibitory percentage of 9.01 %. While this value indicates a modest inhibitory effect against *S. aureus* biofilm, it suggests room for improvement or optimization to enhance the nanoparticles' efficacy. Interestingly, no biofilm inhibitory activity was observed against *S. typhi* and *Proteus* strains, with both showing a 0 % inhibition. In the case of *E. coli*, EE-AuNPs exhibited a substantial biofilm inhibitory percentage of 58.41 %. This result indicates a significant inhibitory effect against *E. coli* biofilm formation, showcasing the potential of EE-AuNPs as an effective agent for combating biofilms produced by this particular strain (Table 3).

Table 2
Biofilm inhibitory percentage of CE-AuNPs and EE-AuNPs.

Biofilm inhibitory percentage (%)				
Test bacteria	*S. aureus*	*S. typhi*	*proteus sp.*	*E. coli*
CE-AuNPs	0	30.6853583	0	19.71014
EE-AuNPs	9.006211	0	0	58.4058

CE-AuNPs: Chloroformic extract loaded on gold nanoparticles, **EE-AuNPs**: Ethyl acetate extract loaded on gold nanoparticles, ***S. aureus***: ***Staphylococcus aureus***, ***E. coli***: *Escherichia coli*, *S. typhi: Salmonella typhi*.

Table 3
Scoring functions of the triterpenes compounds (**1**–**15**) generated from LigandFit docking within the catalytic site of PTP1B.

Compd No.	LigScore1_Dreiding	LigScore2_Dreiding	-PLP1	-PLP2	Jain	-PMF	DOCK_SCORE	Consensus score
9	2.93	3.92	54.52	57.6	1.2	138.84	6.423	5
13	2.28	3.18	22.81	27.26	−2.1	91.54	18.652	5
5	2.16	4.27	39.26	34.83	−2.59	80.15	4.837	4
4	3.06	4.11	40.52	41.49	−0.05	104.47	10.32	2
1	2.92	4.1	38.42	35.29	−1.33	94.22	18.256	1
6	3.86	4.84	53.56	54.33	−2.17	111.69	9.754	1
7	4.6	4.93	42.11	43.66	−0.57	100.44	8.363	1
11	2.09	3.69	46.13	45.82	−0.83	125.68	21.884	1
12	2.54	4.6	56.03	55.68	−1.65	122	19.542	1
15	2.46	3.73	28.36	32.32	−1.15	91.91	4.49	0
2	2.12	4.14	46.62	46.45	−1.08	109.89	0.99	0
3	1.79	3.69	32.28	31.69	−1.31	97.28	12.711	0
8	2.35	3.97	40.99	39.95	−0.22	109.35	4.299	0
10	2.97	4.43	46.98	47.54	−0.56	77.1	18.328	0

4. Molecular modeling studies of bioactive metabolites

4.1. Target identification

To elucidate the molecular target responsible for the anticancer activities of triterpene compounds (**1**–**15**) from CE, we employed the SwissTargetPrediction tool provided by the Swiss Institute of Bioinformatics [34]. Interestingly, all compounds showed good target probability against Protein-tyrosine phosphatase 1B (PTP1B). PTP1B is a drug target for type 2 diabetes mellitus and obesity [35], and it is also a significant target for breast cancer [36]. PTP1B expression is frequently amplified in breast cancer, playing a pivotal role as a cancer promoter by positively or negatively regulating multiple pathways, including Src [37] and rat sarcoma/mitogen activated protein kinase (Ras-MAPK) [38]. PTP1B is an oncogene that promotes cell proliferation, mitosis, adhesion, and invasion [39].

The ability of the triterpenes compounds (1–15) to inhibit PTP1B was not surprising. Several triterpenes with a similar chemical scaffold have been reported as inhibitors of PTP1B with low micromolar affinity. Derivatives of oleanolic acid, a pentacyclic triterpenoid, demonstrated moderate to good inhibitory activities against PTP1B [40]. One chemically modified analogue of oleanolic acid showed an affinity Ki value of 130 nM and exhibited good selectivity over other phosphatases [41]. Cinnamoyl ester and ethyl ether of oleanolic acid showed potent in vitro inhibitory activity and significantly reduced blood glucose levels in an animal model [42]. Triterpenes isolated from the rhizomes of Astilbe koreana inhibited PTP1B with low micromolar IC_{50} values [43]. Dammarane-type triterpenes from hydrolyzate of *Gynostemma pentaphyllum* saponins significantly inhibited the PTP1B enzyme activity in a dose-dependent manner [44,45]. Semi-synthesized derivatives of moronic acid, natural pentacyclic triterpene extracted from Rhus javanica, displayed potent inhibitory activities against PTP1B and displayed an anti-diabetic impact in vivo utilizing a rat model of non-insulin-dependent diabetes mellitus [46]. Ursane-type triterpenoids isolated from the leaves of persimmon (Diospyros kaki) inhibited PTP1B with IC_{50} values ranging from 3.1 to 18.8 μM [47].

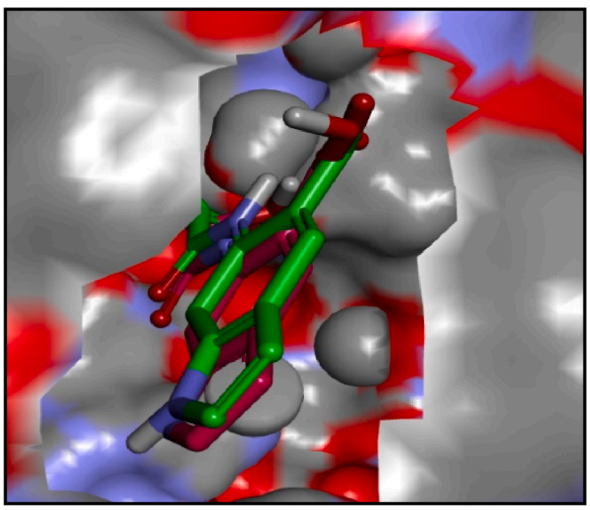

Fig. 9. Alignment of co-crystalized ligand (purple) of PTP1B (PDB code 1C83) and the docked pose (green). (For interpretation of the references to color in this figure legend, the reader is referred to the Web version of this article.)

4.2. Molcular docking

In order to investigate the potential binding interactions of the triterpenes compounds (1–15), we decided to implement molecular docking to elucidate their potential binding to PTP1B and to monitor their interactions. Competitive inhibition is proposed for the targeted compounds (rather than allosteric inhibition) since an experimental validation of structurally similar triterpenes showed competitive behavior and potential binding to an extended binding pocket (site B) adjacent to the catalytic site A [40,46]. The predicted binding of the co-crystalized ligand for PTP1B (PDB code 1C83) was determined to validate the docking protocol. As shown in Fig. 9, the docked and the co-crystalized poses are aligned with a root-mean square deviation (RMSD) of 0.726 Å.

All compounds were successfully docked with good docking scoring functions (Table 3). Consensus scoring from 7 scoring functions was subsequently applied to rank the docked compounds. It involves combining multiple scoring functions to assess the binding affinity between a ligand and a target protein, aiming to improve the accuracy and reliability of the docking results by considering different aspects of the molecular interaction [48]. Compounds 9 and 13 showed the highest consensus scoring among the successfully docked compounds, with a score of 5 (Table 3). The predicted binding poses of compounds 9 and 13 are nearly identical, where the two compounds cap the entrance of the catalytic binding site. At the same time, the β-hydroxyester side chain is injected deep within the catalytic site through van der Waals interactions and hydrogen bonding (Fig. 10). Compound 9 showed hydrogen bonding interaction with LYS120, π-lone pair interaction with TYR46, and van der Waals interactions with ALA217, VAL49, PHE182, CYS215, ILE219, GLY220, and GLY259 (Fig. 10A). Similarly, the compound 13 formed hydrogen bonding interaction with LYS120 and TYR46 and van der Waals interactions with PHE182, ALA217, CYS215, ILE219, and GLY220 (Fig. 10B).

4.3. Molecular dynamics (MD)

Docking alone needs to offer adequate information regarding binding affinity or interaction stability. Therefore, the highest-ranked docked compounds (9 and 13) complexed with PTP1B underwent 100 ns classical MD simulations. The RMSD analysis indicated that stability was achieved for the complexes and individual ligands within the PTP1B catalytic site within the first 20 ns of the simulation, with deviations remaining below 3 Å after 50 ns of the simulation period (Fig. 11A). The complex stability was supported by Root Mean Square Fluctuation (RMSF) analysis, which provides information about the flexibility or mobility of individual atoms within a protein throughout the simulation. The RMSF plot demonstrated no sudden fluctuations in any complexes, with RMSF lying within 0.43–2.87 Å for the PTP1B-9 complex and 0.37–2.56 Å for the PTP1B-13 complex (Fig. 11B).

Furthermore, the interactions of compounds 9 and 13 with PTP1B and their corresponding occupancies were calculated.

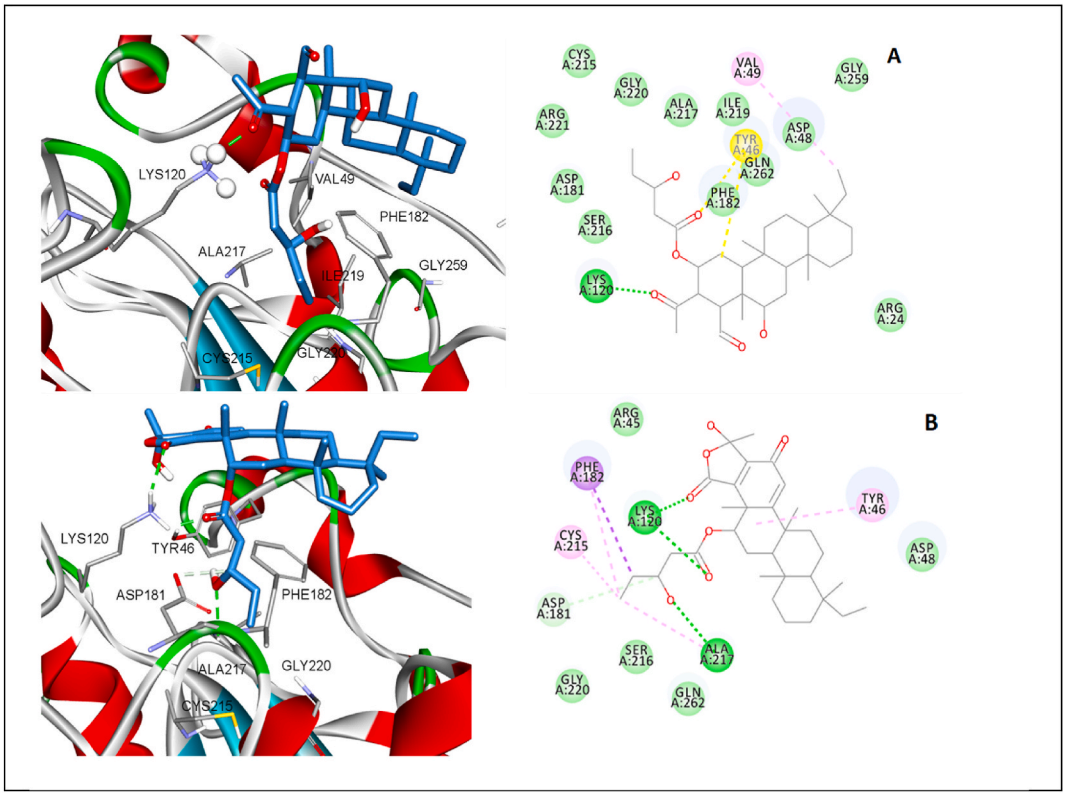

Fig. 10. The 3D and 2D representation of the docked poses of compounds **9** (A) and **13** (B).

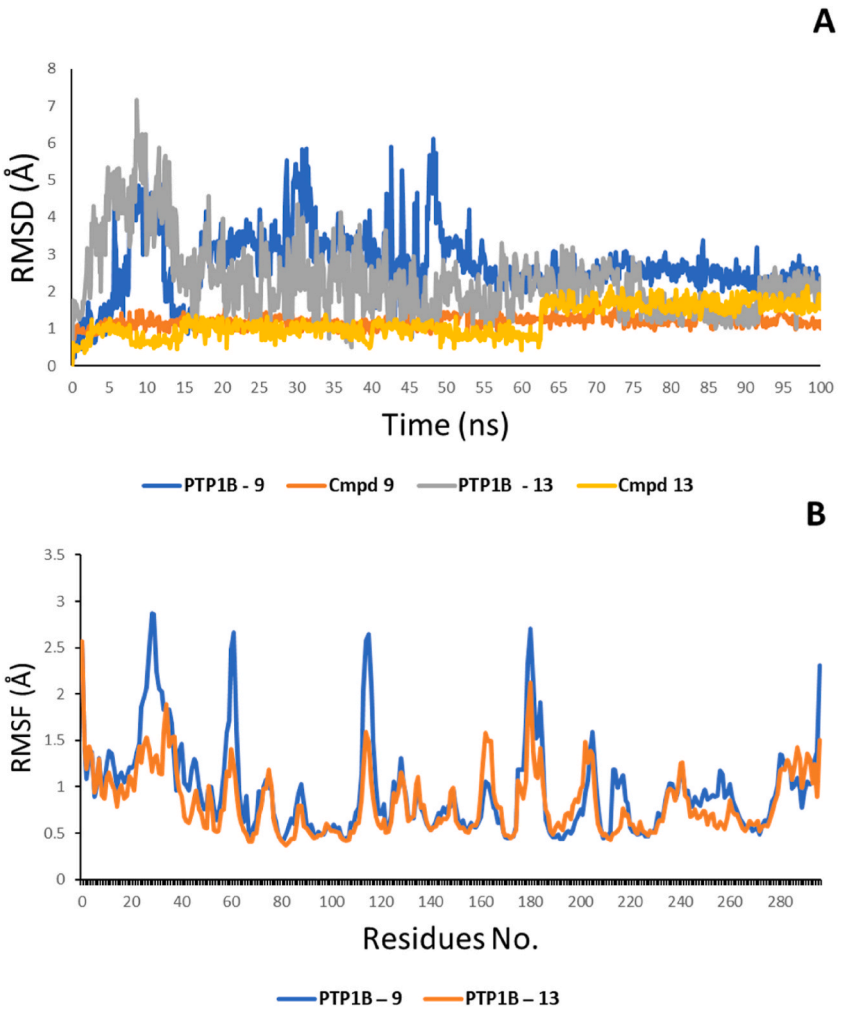

Fig. 11. The binding of compounds **9** and **13** with PTP1B. (A) The RMSD plot of the ligands alone and with PTP1B (B) The RMSF plot showing the fluctuation of individual amino acids after ligand binding.

Compound 9 interacted with LYS120 and TYR46 for 57 % and 49 % of the simulation time, respectively. In contrast, compound 13 exhibited higher occupancy with the same amino acids, accounting for 74 % and 82 % of the simulation time, respectively (Fig. 12A and B).

To evaluate the binding affinity of compounds 9 and 13 to PTP1B, binding free energy was calculated using CHARMm-based energy and Generalized Born with a simple Switching (GBSW). The CHARMm/GBSW calculation showed that compound 13 had a higher binding affinity for PTP1B with an average binding energy of −30.51 kcal/mol, while compound 9had −24.28 kcal/mol.

Our comprehensive research, which included docking studies and MD simulations of compounds 9 and 13, unequivocally demonstrated their potential to competitively inhibit PTP1B. This finding provides a compelling explanation for the anticancer activities of triterpenes compounds extracted from *P. lamellosa*.

5. Experimental

5.1. Collection of marine sponge

The marine sponge (1 kg) was collected in November 2023 from Hurghada along the Red Sea Coast (27°15048″ north (N), 33°4903” east (E)) at a depth of 7 m. A voucher sample (NUB-009/2023) was reserved at the Pharmacognosy Department, Faculty of Pharmacy, Nahda University in Bemi-Suef, Egypt.

5.2. Preparation of extracts

Sponge material was cut into small pieces and then subjected to ultrasonic-assisted ethanol extraction, as mentioned on page S1

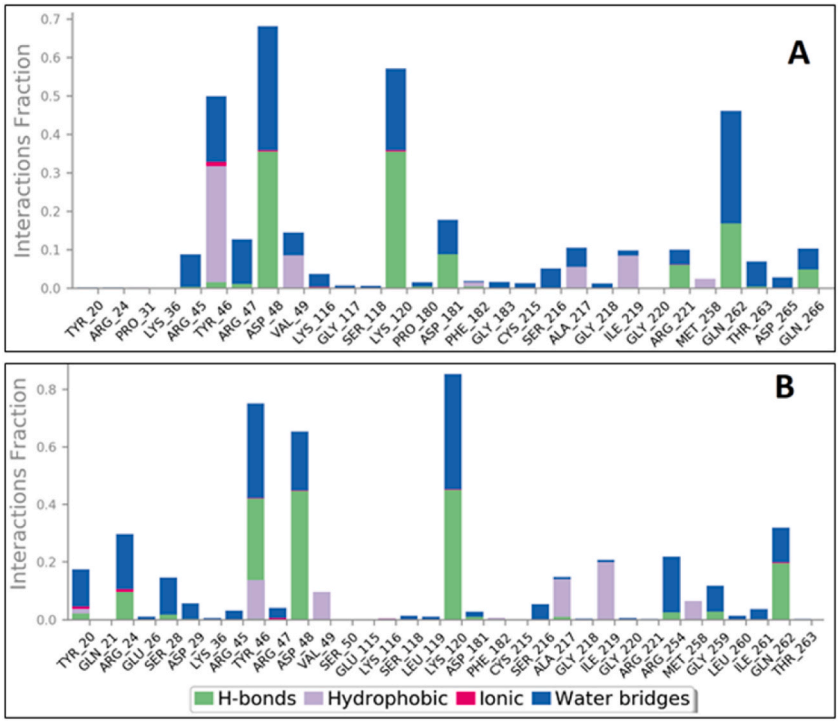

Fig. 12. The critical interactions of compound 9 (A) and compound 13 (B) with PTP1B throughout the simulation time.

(supplementary material).

5.3. Metabolomic analysis

According to the findings outlined by Musa et al. (2022) [49], the obtained extracts were exposed to metabolic analysis using liquid chromatography-high resolution electrospray ionization mass spectrometry (LC-HRESIMS). The LC-HRESIMS approach specifics are available on supplementary data page S1.

5.4. Preparation of AuNPs

The green synthesis of gold nanoparticles was conducted according to the methodology described by El-Ghorab et al., 2022 [50], Page S3.

5.5. Characterization of AuNPs

All basic techniques utilized in gold Nanoparticle characterization, including UV spectroscopy, X-ray diffraction (XRD) studies, Fourier-transform infrared, transmission electron microscopy analysis (TEM) spectroscopy (FTIR), and Scanning electron microscope (SEM), are available on supplementary data pages S4 and S5.

5.6. Cytotoxicity assay of AuNPs-loaded P. lamellosa extracts

The anti-proliferative activity of the prepared CE (chloroformic extract), EE (ethyl acetate extract), and AuNPs was described in detail in supplementary data page S6.

5.7. Determination of the antimicrobial activity of AuNPs-loaded P. lamellosa extracts

The antimicrobial tests used to measure the nanoparticles' antimicrobial activities of the tested extracts (final concentration of 50 μg/ml) against the test organisms are summarized in supplementary data page S5.

5.8. Anti-biofilm activity of AuNPs-loaded P. lamellosa extracts

The anti-biofilm activity of the prepared CE (chloroformic extract), EE (ethyl acetate extract), and AuNPs extracts (final

concentration of 50 μg/ml)was described in detail in supplementary data page S6.

5.9. Molecular modeling of bioactive metabolites

The molecular docking and Molecular Dynamic (MD) Simulation experiments of the most promising metabolites are detailed in supplementary data pages S7 and S8.

5.10. Statistical analysis

Results were analyzed statistically using the computerized program SPSS software, version 20, for Windows. The one-way analysis of variance (ANOVA) test was followed by the Duncan test. Data were represented as mean ± SE values.

6. Conclusions

The LC–HRESIMS-assisted chemical profiling utilized in the analysis of P. lamellosa extract in this current investigation demonstrated the abundance of terpenoids in the CE fraction, brominated aromatic ethers, and sulfated fatty amides in the EE fraction. Incorporating those extracts in the green creation of metal nanoparticles (MNPs) led to the preparation of bioactive AuNPs that exerted remarkable anticancer characteristics against estrogen-sensitive human breast cancer cell lines and antibacterial effect, especially against E. coli. Moreover, EE-AuNPs exert a remarkable anti-biofilm activity against E. coli. A plethora of sisterterpenes and triterpenes were suggested to be the probable active chemical compounds after conducting molecular modeling studies of the putatively identified metabolites in the sponge extract. Additionally, it was proposed that these active metabolites might mediate targeting of PTP1B in order to exert their anti-breast cancer effect.

Funding

The authors are thanks to Researchers Supporting Project number (RSP2024R504), King Saud University, Riyadh, Saudi Arabia.

CRediT authorship contribution statement

Sultan Aati: Writing – original draft, Methodology. **Hanan Y. Aati:** Supervision, Resources, Funding acquisition. **Sherine El-Shamy:** Visualization, Software. **Mohammad A. Khanfar:** Writing – original draft, Methodology, Formal analysis, Data curation. **Mohamed A.Ghani A.Naeim:** Resources. **Ahmed A. Hamed:** Writing – original draft, Formal analysis. **Mostafa E. Rateb:** Writing – review & editing, Conceptualization. **Hossam M. Hassan:** Writing – review & editing, Project administration, Data curation, Conceptualization. **Mahmoud A. Aboseada:** Writing – original draft, Formal analysis.

Declaration of competing interest

The authors declare that they have no known competing financial interests or personal relationships that could have appeared to influence the work reported in this paper.

Acknowledgments

-The authors would like to thank the Researchers Supporting Project number (RSP2024R504), King Saud University, Riyadh, Saudi Arabia.

Appendix A. Supplementary data

Supplementary data to this article can be found online at https://doi.org/10.1016/j.heliyon.2024.e34000.

References

[1] H.K. Matthews, C. Bertoli, R.A.M. de Bruin, Cell cycle control in cancer, Nat. Rev. Mol. Cell Biol. 23 (2022) 74–88.
[2] D. Hanahan, Hallmarks of cancer: new dimensions, Cancer Discov. 12 (2022) 31–46.
[3] J. Ferlay, M. Colombet, I. Soerjomataram, D.M. Parkin, M. Piñeros, A. Znaor, F. Bray, Cancer statistics for the year 2020: an overview, Int. J. Cancer 149 (2021) 778–789.
[4] A. Desai, C. Scheckel, C.J. Jensen, J. Orme, C. Williams, N. Shah, K. Leventakos, A.A. Adjei, Trends in Prices of drugs used to treat metastatic non–small cell lung cancer in the US from 2015 to 2020, JAMA Netw. Open 5 (2022) e2144923.
[5] B.S. Chhikara, K. Parang, Global Cancer Statistics 2022: the trends projection analysis, Chem. Biol. Lett. 10 (2023) 451.
[6] L. Peng, Z. Wang, J. Stebbing, Z. Yu, Novel immunotherapeutic drugs for the treatment of lung cancer, Curr. Opin. Oncol. 34 (2022) 89–94.
[7] M. Xu, R. Peng, Q. Min, S. Hui, X. Chen, G. Yang, S. Qin, Bisindole natural products: a vital source for the development of new anticancer drugs, Eur. J. Med. Chem. 243 (2022) 114748.

[8] A. Zigrossi, L.K. Hong, R.C. Ekyalongo, C. Cruz-Alvarez, E. Gornick, A.M. Diamond, I. Kastrati, SELENOF is a new tumor suppressor in breast cancer, Oncogene 41 (2022) 1263–1268.
[9] F. Ye, S. Dewanjee, Y. Li, N.K. Jha, Z.-S. Chen, A. Kumar, Vishakha, T. Behl, S.K. Jha, H. Tang, Advancements in clinical aspects of targeted therapy and immunotherapy in breast cancer, Mol. Cancer 22 (2023) 105.
[10] M.A. Salam, M.Y. Al-Amin, M.T. Salam, J.S. Pawar, N. Akhter, A.A. Rabaan, M.A.A. Alqumber, Antimicrobial resistance: a growing serious threat for global public health, in: Healthcare, MDPI, 2023, p. 1946.
[11] F.C. Tenover, Mechanisms of antimicrobial resistance in bacteria, Am. J. Med. 119 (2006) S3–S10.
[12] J. Williams-Nguyen, J.B. Sallach, S. Bartelt-Hunt, A.B. Boxall, L.M. Durso, J.E. McLain, R.S. Singer, D.D. Snow, J.L. Zilles, Antibiotics and antibiotic resistance in agroecosystems: state of the science, J. Environ. Qual. 45 (2016) 394–406.
[13] B. Khameneh, R. Diab, K. Ghazvini, B.S.F. Bazzaz, Breakthroughs in bacterial resistance mechanisms and the potential ways to combat them, Microb. Pathog. 95 (2016) 32–42.
[14] N.T. Telang, Natural products as drug candidates for breast cancer, Oncol. Lett. 26 (2023) 1–8.
[15] S.A. Mobeen, P. Saxena, A.K. Jain, R. Deval, K. Riazunnisa, D. Pradhan, Integrated bioinformatics approach to unwind key genes and pathways involved in colorectal cancer, J. Cancer Res. Therapeut. (2023).
[16] M. Kiranmayee, N. Rajesh, M. Vidya Vani, H. Khadri, A. Mohammed, S. V Chinni, G. Ramachawolran, K. Riazunnisa, A.Y. Moussa, Green synthesis of Piper nigrum copper-based nanoparticles: in silico study and ADMET analysis to assess their antioxidant, antibacterial, and cytotoxic effects, Front. Chem. 11 (2023) 1218588.
[17] A. Almatroudi, H. Khadri, M. Azam, A.H. Rahmani, F.K. Al Khaleefah, R. Khateef, M.A. Ansari, K.S. Allemailem, Antibacterial, antibiofilm and anticancer activity of biologically synthesized silver nanoparticles using seed extract of Nigella sativa, Processes 8 (2020) 388.
[18] K.S. Allemailem, H. Khadri, M. Azam, M.A. Khan, A.H. Rahmani, F. Alrumaihi, R. Khateef, M.A. Ansari, E.A. Alatawi, M.H. Alsugoor, Ajwa-dates (phoenix dactylifera)-mediated synthesis of silver nanoparticles and their anti-bacterial, anti-biofilm, and cytotoxic potential, Appl. Sci. 12 (2022) 4537.
[19] A. El-Demerdash, A.G. Atanasov, O.K. Horbanczuk, M.A. Tammam, M. Abdel-Mogib, J.N.A. Hooper, N. Sekeroglu, A. Al-Mourabit, A. Kijjoa, Chemical diversity and biological activities of marine sponges of the genus Suberea: a systematic review, Mar. Drugs 17 (2019) 115.
[20] H. Zhang, M. Dong, H. Wang, P. Crews, Secondary metabolites from the marine sponge genus Phyllospongia, Mar. Drugs 15 (2017) 12.
[21] L.C. Chang, S. Otero-Quintero, G.M. Nicholas, C.A. Bewley, Phyllolactones A–E: new bishomoscalarane sesterterpenes from the marine sponge Phyllospongia lamellosa, Tetrahedron 57 (2001) 5731–5738.
[22] M.H.A. Hassan, M.E. Rateb, M. Hetta, T.A. Abdelaziz, M.A. Sleim, M. Jaspars, R. Mohammed, Scalarane sesterterpenes from the Egyptian Red Sea sponge Phyllospongia lamellosa, Tetrahedron 71 (2015) 577–583.
[23] K.-H. Lai, Y.-C. Liu, J.-H. Su, M. El-Shazly, C.-F. Wu, Y.-C. Du, Y.-M. Hsu, J.-C. Yang, M.-K. Weng, C.-H. Chou, Antileukemic scalarane sesterterpenoids and meroditerpenoid from Carteriospongia (Phyllospongia) sp., induce apoptosis via dual inhibitory effects on topoisomerase II and Hsp90, Sci. Rep. 6 (2016) 36170.
[24] S.M. Lee, N.-H. Kim, S. Lee, Y.N. Kim, J.D. Heo, E.J. Jeong, J.-R. Rho, Deacetylphylloketal, a new phylloketal derivative from a marine sponge, genus Phyllospongia, with potent anti-inflammatory activity in in vitro co-culture model of intestine, Mar. Drugs 17 (2019) 634.
[25] M.W.B. McCulloch, T.S. Bugni, G.P. Concepcion, G.S. Coombs, M.K. Harper, S. Kaur, G.C. Mangalindan, M.M. Mutizwa, C.A. Veltri, D.M. Virshup, Carteriosulfonic acids A– C, GSK-3β inhibitors from a carteriospongia sp, J. Nat. Prod. 72 (2009) 1651–1656.
[26] H. Khan, H. Ullah, M. Martorell, S.E. Valdes, T. Belwal, S. Tejada, A. Sureda, M.A. Kamal, Flavonoids nanoparticles in cancer: treatment, prevention and clinical prospects, in: Semin. Cancer Biol., Elsevier, 2021, pp. 200–211.
[27] P. de la Torre, M.J. Pérez-Lorenzo, Á. Alcázar-Garrido, A.I. Flores, Cell-based nanoparticles delivery systems for targeted cancer therapy: lessons from anti-angiogenesis treatments, Molecules 25 (2020) 715.
[28] D. Ion, A.-G. Niculescu, D.N. Păduraru, O. Andronic, F. Mușat, A.M. Grumezescu, A. Bolocan, An up-to-date review of natural nanoparticles for cancer management, Pharmaceutics 14 (2021) 18.
[29] G.P. Concepcion, A.R.J. Anas, M.A. Azcuna, Anticancer compounds from Philippine marine organisms act on major pathways in cancer, Philipp, Sci. Lett. 7 (2014) 207–227.
[30] D. Karati, K.K. Shaoo, K.R. Mahadik, D. Kumr, Glycogen synthase kinase-3β inhibitors as a novel promising target in the treatment of cancer: medicinal Chemistry Perspective, Results Chem (2022) 100532.
[31] L. Schmitt, I. Hinxlage, P.A. Cea, H. Gohlke, S. Wesselborg, 40 Years of research on polybrominated diphenyl ethers (PBDEs)—a historical overview and newest data of a promising anticancer drug, Molecules 26 (2021) 995.
[32] A. Nasser Alahmari, S. A Hassoubah, B. Ali Alaidaroos, Sponges-associated marine bacteria as sources of antimicrobial compounds, Nov. Res. Microbiol. J. 6 (2022) 1742–1767.
[33] D. Ki, M.D. Awouafack, C.P. Wong, H.M. Nguyen, Q.M. Thai, L.H. Ton Nu, H. Morita, Brominated diphenyl ethers including a new tribromoiododiphenyl ether from the Vietnamese marine sponge Arenosclera sp. and their antibacterial activities, Chem. Biodivers. 16 (2019) e1800593.
[34] A. Daina, O. Michielin, V. Zoete, SwissTargetPrediction: updated data and new features for efficient prediction of protein targets of small molecules, Nucleic Acids Res. 47 (2019) W357–W364.
[35] H. Cho, Protein tyrosine phosphatase 1B (PTP1B) and obesity, Vitam. Horm. 91 (2013) 405–424.
[36] S. Liao, J. Li, L. Yu, S. Sun, Protein tyrosine phosphatase 1B expression contributes to the development of breast cancer, J. Zhejiang Univ. B. 18 (2017) 334–342.
[37] J.D. Bjorge, A. Pang, D.J. Fujita, Identification of protein-tyrosine phosphatase 1B as the major tyrosine phosphatase activity capable of dephosphorylating and activating c-Src in several human breast cancer cell lines, J. Biol. Chem. 275 (2000) 41439–41446.
[38] N. Dubé, A. Cheng, M.L. Tremblay, The role of protein tyrosine phosphatase 1B in Ras signaling, Proc. Natl. Acad. Sci. USA 101 (2004) 1834–1839.
[39] M. Yu, Z. Liu, Y. Liu, X. Zhou, F. Sun, Y. Liu, L. Li, S. Hua, Y. Zhao, H. Gao, PTP 1B markedly promotes breast cancer progression and is regulated by miR-193a-3p, FEBS J. 286 (2019) 1136–1153.
[40] S. Qian, H. Li, Y. Chen, W. Zhang, S. Yang, Y. Wu, Synthesis and biological evaluation of oleanolic acid derivatives as inhibitors of protein tyrosine phosphatase 1B, J. Nat. Prod. 73 (2010) 1743–1750.
[41] Y.-N. Zhang, W. Zhang, D. Hong, L. Shi, Q. Shen, J.-Y. Li, J. Li, L.-H. Hu, Oleanolic acid and its derivatives: new inhibitor of protein tyrosine phosphatase 1B with cellular activities, Bioorg. Med. Chem. 16 (2008) 8697–8705.
[42] J.J. Ramírez-Espinosa, M.Y. Rios, P. Paoli, V. Flores-Morales, G. Camici, V. de la Rosa-Lugo, S. Hidalgo-Figueroa, G. Navarrete-Vázquez, S. Estrada-Soto, Synthesis of oleanolic acid derivatives: in vitro, in vivo and in silico studies for PTP-1B inhibition, Eur. J. Med. Chem. 87 (2014) 316–327.
[43] M. Na, L. Cui, B.S. Min, K. Bae, J.K. Yoo, B.Y. Kim, W.K. Oh, J.S. Ahn, Protein tyrosine phosphatase 1B inhibitory activity of triterpenes isolated from Astilbe koreana, Bioorg. Med. Chem. Lett. 16 (2006) 3273–3276.
[44] J.-Q. Xu, Q. Shen, J. Li, L.-H. Hu, Dammaranes from Gynostemma pentaphyllum and synthesis of their derivatives as inhibitors of protein tyrosine phosphatase 1B, Bioorg. Med. Chem. 18 (2010) 3934–3939.
[45] X.-S. Zhang, X.-L. Bi, J.-Q. Cao, X.-C. Xia, Y.-P. Diao, Y.-Q. Zhao, Protein tyrosine phosphatase 1B inhibitory effect by dammarane-type triterpenes from hydrolyzate of total Gynostemma pentaphyllum saponins, Bioorg. Med. Chem. Lett. 23 (2013) 297–300.
[46] L. Cerón-Romero, P. Paoli, G. Camici, V. Flores-Morales, M.Y. Rios, J.J. Ramírez-Espinosa, S. Hidalgo-Figueroa, G. Navarrete-Vázquez, S. Estrada-Soto, In vitro and in silico PTP-1B inhibition and in vivo antidiabetic activity of semisynthetic moronic acid derivatives, Bioorg. Med. Chem. Lett. 26 (2016) 2018–2022.
[47] P.T. Thuong, C.H. Lee, T.T. Dao, P.H. Nguyen, W.G. Kim, S.J. Lee, W.K. Oh, Triterpenoids from the leaves of Diospyros kaki (persimmon) and their inhibitory effects on protein tyrosine phosphatase 1B, J. Nat. Prod. 71 (2008) 1775–1778.

[48] P.S. Charifson, J.J. Corkery, M.A. Murcko, W.P. Walters, Consensus scoring: a method for obtaining improved hit rates from docking databases of three-dimensional structures into proteins, J. Med. Chem. 42 (1999) 5100–5109.
[49] A. Musa, M.A. Abdelgawad, M.E. Shaker, A.H. El-Ghorab, D.G.T. Parambi, A.A. Hamed, A.M. Sayed, H.M. Hassan, M.A. Aboseada, Screening and molecular docking of bioactive metabolites of the Red Sea sponge callyspongia siphonella as potential antimicrobial agents, Antibiotics 11 (2022) 1682.
[50] A.H. El-Ghorab, F.A. Behery, M.A. Abdelgawad, I.H. Alsohaimi, A. Musa, E.M. Mostafa, H.A. Altaleb, I.O. Althobaiti, M. Hamza, M.H. Elkomy, LC/MS profiling and gold nanoparticle formulation of major metabolites from origanum majorana as antibacterial and antioxidant potentialities, Plants 11 (2022) 1871.